Int. J. Heat Mass Transfer. Vol. 3, pp. 255–265. Pergamon Press 1961. Printed in Great Britain.

VELOCITY AND TEMPERATURE PROFILES IN A WALL JET

R. A. SEBAN* and L. H. BACK†

(*Received* 8 *February* 1961, *in revised form* 24 *May* 1961)

Abstract—Conditions approximating those of the wall jet have been obtained by operating a system, involving tangential air injection into a turbulent boundary layer, with very low values of the free stream velocity. Under such conditions the flow is essentially produced by the injected air and measurement of the velocity profiles shows correspondence to the theory for the turbulent wall jet. With some alternation of the eddy diffusivity of that theory the measured temperature profiles can also be predicted and these, together with the velocity profiles, are shown to agree generally with the measured values of the adiabatic wall temperature. The measured heat transfer coefficients are related to the hydrodynamic characteristics by a formulation of the Colburn type.

Résumé—Des conditions se rapprochant de celles du jet à la paroi ont été réalisées avec un dispositif compartant une injection tangentielle d'air dans une couche limite turbulente, les vitesses de l'écoulement libre étant très basses. Dans de telles conditions, l'écoulement est essentiellement produit par l'air injecté et la mesure des profils de vitesses est en accord avec la théorie du jet turbulent à la paroi. Les profils de température mesurés se retrouvent également par cette théorie si l'on fait quelques corrections sur la diffusivité turbulente; ces profils de vitesse et de température sont généralement en bon accord avec la température de paroi adiabatique mesurée. Les mesures des coefficients de transmission de chaleur sont reliées aux caractéristiques hydrodynamiques par une formule du type Colburn.

Zusammenfassung—Durch tangentiales Einblasen von Luft sehr kleiner Freistromgeschwindigkeit in die turbulente Grenzschicht wurden angenähert die bei einem Schlitz auftretenden Verhältnisse erreicht. Die Strömung wird dabei im wesentlichen von der eingeblasenen Luft hervorgerufen und Messungen des Geschwindigkeitsprofils zeigen Übereinstimmung mit der Theorie für turbulente Schlitzströmungen. Nach Änderung der turbulenten Austauschgrösse der Theorie können auch die gemessenen Temperaturprofile vorherbestimmt werden und stimmen, zusammen mit den Geschwindigkeitsprofilen, im Allgemeinen mit den ermittelten Werten der adiabaten Wandtemperatur überein. Die gemessenen Wärmeübergangskoeffizienten sind nach einer Formulierung von Colburn auf die kennzeichnenden hydrodynamischen Grössen bezogen.

Аннотация—С помощью системы, обеспечнвающей вдув воздуха по касательной в турбулентный пограничный слой, получены условия, аппроксимирующие условия для струи вблизи стенкн (при очень малых значениях скорости невозмущённого потока). При таких условиях поток, по существу, создаётся здуваемым воздухом, а пзмеренные профили скорости свидетельствуют о соответствии их с теорией турбулентной струи вблизи стенки. Если несколько изменить принятый в этой теории коэффициент диффузии вихря, то измеренные температурные профили могут также быть заданы. Показано, что вместе с профилями скорости они, в общем, согласуются с измеренными величинами температуры адиабатической стенки. Коэффициенты переноса тепла связаны с гидродинамическими характеристиками при помощи аналогии Колбэрна.

NOMENCLATURE

$a, b,$ defined in equations (1) or (2);
$c_p,$ specific heat at constant pressure;
$h,$ local heat transfer coefficient;
$s,$ injection slot height;
$t,$ temperature above free stream, °F; t_s injection air, t_1 free stream, t_a adiabatic wall temperature;
$T,$ absolute temperature, °R;
$u,$ velocity; u_s injection air, u_1 free stream, u_m maximum velocity, U reference velocity;

* Professor of Mechanical Engineering, University of California, Berkeley, California.

† Research Assistant, Institute of Engineering Research, University of California, Berkeley, California.

v, velocity;
x, distance downstream from slot;
x_0, positive distance between the slot and the effective origin of the jet;
y, distance from wall.

Greek symbols

$\xi = x + x_0$, distance downstream from the effective origin of the jet;
δ, distance from wall to the point in the outer region at which $u = u_m/2$;
δ_m, distance from wall to velocity maximum;
$\delta_t = \delta - \delta_m$, distance from velocity maximum to the point where $u = u_m/2$;
$\zeta = y/\delta$, dimensionless distance from wall;
η, similarity variable defined in equation (4);
α, velocity profile parameter;
ν, kinematic viscosity;
ϵ, diffusivity;
τ_0, shearing stress at wall;
σ, Prandtl number;
ρ, density.

Subscripts

s, injection air;
1, free stream;
a, adiabatic wall.

INTRODUCTION

RESULTS have been presented [1] in a previous report for the heat transfer coefficient and for the effectiveness that were obtained from a system involving the tangential injection of air into the turbulent boundary layer produced by an air stream flowing over a plate. This apparatus, which was essentially a model of a film cooling system, was operated with both high and low ratios of the injection velocity to the free stream velocity, and for the high ratios the results for the effectiveness and for the heat transfer coefficient were found to correspond to the earlier results of Jakob [2] that were obtained on a similar system in which the free stream velocity was zero. Without free stream velocity, the flow situation is that of the wall jet and that is the focus of the present consideration even though the free stream velocity could not be eliminated completely in the system from which the present results were obtained. It was the availability of this system for the provision of some detailed hydrodynamic and thermal characteristics that produced the present results, which demonstrate that the major characteristics of the flow agree with the theory of the wall jet as given by Glauert [3] and that the effectiveness and the heat transfer coefficients that have already been correlated empirically do agree with the consequences of that theory.

The system shown in Fig. 1, from which were obtained the present results, consisted of a test surface, 12 in wide and 18 in long, which was one side of the 4 in $\times$ 12 in rectangular test section of a small, once through, wind tunnel. The injection slot, variable in height, spanned the 12 in width of the test surface and was located at its upstream edge, just downstream of the tunnel nozzle. There existed provisions for heating the injection air, heating the plate, and for the determination of the necessary temperatures

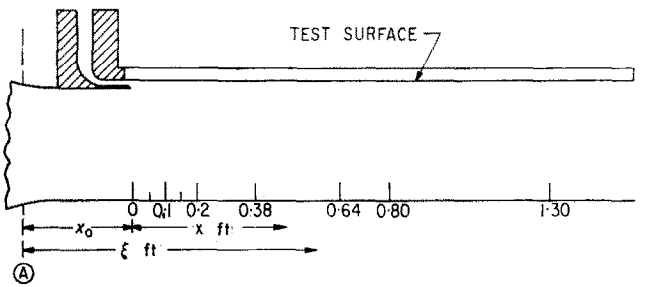

FIG. 1. Slot and test section. Point "A" is the effective origin of the jet.

and pressures. The low free stream velocities that existed for the operation that is considered here were obtained with the tunnel blower inoperative and the main stream flow was also restricted to the point of incipient back flow in the test section.

THE WALL JET

Glauert [3] achieved an analytical specification of the wall jet for both laminar and turbulent flow, for the latter on the basis of a near similarity in which the velocity profiles are relatively invariable for given orders of the Reynolds number. The essential nature of these profiles is characterized by a parameter α, indicative of the proportional extent of the inner flow, between the wall and the velocity maximum, to that of the outer flow between the velocity maximum and the stationary fluid far from the wall. Fig. 2 shows the nature of the velocity profile of the flow, which begins at a source and proceeds downstream, with the maximum velocity diminishing according to a power law, $u_m \sim \xi^a$. The width of the layer, too, follows a power law, $\delta \sim \xi^b$ and the exponents a and b are related to the parameter α in two possible and similar ways,

$$\left.\begin{aligned} a &= \frac{-4\alpha}{5+4\alpha} \\ b &= \frac{4+4\alpha}{5+4\alpha} \end{aligned}\right\} \qquad (1)$$

or

$$\left.\begin{aligned} a &= -\frac{\alpha}{1+\alpha} \\ b &= 1 \end{aligned}\right\}. \qquad (2)$$

The analysis gives the local velocity in terms of a reference velocity U, not easily defined, and an additional parameter λ which depends on α.

$$u = U\left[\frac{4-4b}{\lambda}\left(\frac{U\xi}{\nu}\right)^{4-5b}\frac{\mathrm{d}f}{\mathrm{d}\eta}\right]. \qquad (3)$$

The function f, associated with the stream function, is of course the essential result of the similarity solution. The similarity variable, η, is

$$\eta = \frac{4-4b}{\lambda}\,\frac{yU}{\nu}\left(\frac{U\xi}{\nu}\right)^{-b}. \qquad (4)$$

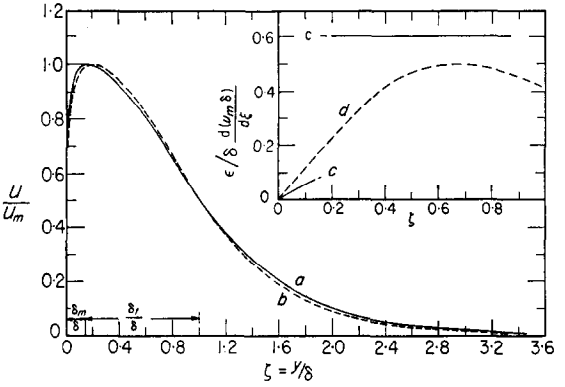

FIG. 2. Velocity profiles from Glauert's theory. Curve a is the profile for $\alpha = 1{\cdot}2$, curve b for $\alpha = 1{\cdot}3$. The inset shows the distribution of the diffusivity and curve c is that corresponding to the velocity distribution for $\alpha = 1{\cdot}2$. Curve d is a deduction based on the measured temperature profiles.

Fig. 2 shows $\mathrm{d}f/\mathrm{d}\eta$ as a function of η, through co-ordinates which are actually

$$\frac{\mathrm{d}f}{\mathrm{d}\eta}\Big/\left(\frac{\mathrm{d}f}{\mathrm{d}\eta}\right)_m$$

as a function of η/η_δ, with δ being the distance from the wall to that point in the outer region at which the velocity is half of the maximum value; this is the distance most precisely determined by the experimental results. The figure defines also two other distances that are significant, that from the wall to the velocity maximum, δ_m, and δ_t from the velocity maximum to the point where $u = u_m/2$. The flatness of the experimental profile near the velocity maximum makes the latter distances hard to define experimentally, as revealed by the typical theoretical profiles of Fig. 2.

Primarily because of later concern with the temperature profiles it is important to specify the eddy diffusivity from which were predicted the velocity profiles. Since similarity is unattainable if molecular transport is included precisely, the diffusivity ϵ is presumed to include the molecular effects to the extent they are compatible with similarity. A convenient form for illustration gives the diffusivity in the form produced by integration of the momentum equation

$$\frac{\epsilon\xi}{u_m\delta^2(a+b)} = \frac{\epsilon}{\delta[\mathrm{d}(u_m\delta)/\mathrm{d}\xi]}$$

$$= \left[-\left(\frac{2a+b}{a+b}\right)\int_\xi^\infty F'^2\,\mathrm{d}\xi - FF'\right]\frac{1}{F'} \qquad (5)$$

where $F' = u/u_m$ and $\zeta = y/\delta$.

The values of the diffusivity contained on Fig. 2 were evaluated from equation (5) in the outer region but near the wall accuracy required the use of the alternative specification of Ref. 3. The constant value in the outer region can also be specified as 0·85 $(u_m\delta/\epsilon) = 1/\kappa$, so that $\kappa = 0{\cdot}72\,(a+b)\delta/\xi$ and the constant value of κ implied for the outer region is realized if $b = 1$.

VELOCITY PROFILES

Figure 3 shows the experimental velocity profiles obtained downstream of a slot 0·250 inch in height, at seven downstream positions, to reveal that essential similarity was obtained at the station at 0·642 ft ($x/s = 37{\cdot}0$) and beyond. The profile at $x = 0{\cdot}38$ ($x/s = 18{\cdot}3$) is close to these profiles and in fact gives the best correspondence with Glauert's prediction, while the downstream profiles agree with that of Sigalla [4], obtained experimentally on a wall jet. This points to the possibility that the diffusivity in the outer region may be slightly lower than that assumed in the theory.

Figure 4 presents the experimental profiles obtained with a 0·063 in slot for two different injection velocities. The profiles for the injection velocity of 211 ft/s agree better with the theory than do those for the 0·25 in slot, shown on Fig. 3. Only the profile for $x = 0{\cdot}05$ ft ($x/s = 9{\cdot}6$) shows a marked departure and that at the next station, $x/s = 29$, reveals similarity and agreement with the theory. Similar results exist for the lower injection velocity, except for a departure of the profile at the last station, but there the velocities were very low and the accuracy of the determination much diminished. Generally the results for the smaller slot correspond better with the theory, though the results for the larger slot are not inferior and all the profiles support the theory even in the present case in which the finite free stream velocity terminates the profiles in the outer region of the flow. The influence of the free stream flow is indicated to be small even for ratios u_1/u_m as large as 0·40.

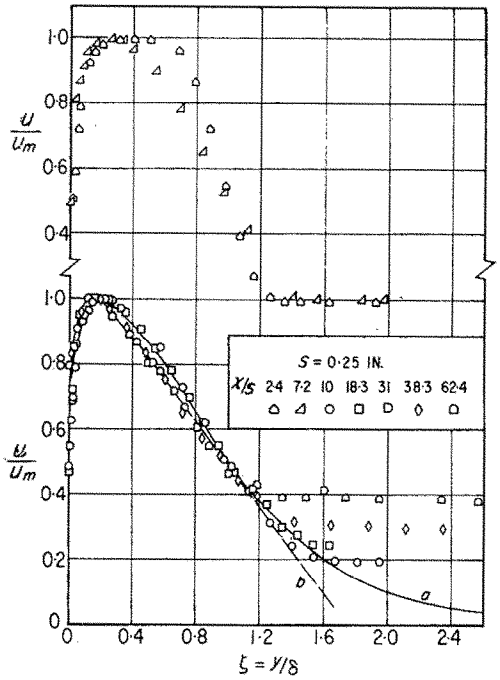

FIG. 3. Velocity profiles for the 0·25 in slot. Curve *a* is the same curve of Fig. 2, curve *b* is the result of Sigalla [4]. The slot Reynolds number was of the order of 6850. Quantities associated with the profiles are as follows.

x/s	u_1 (ft/s)	u_s (ft/s)	u_m (ft/s)	δ (in)	$u_m\delta/\nu$
2·4	9	56	60	0·27	7920
7·2	11	56	56	0·35	9650
10·0	8	58	52	0·37	9400
18·3	9	58	45	0·51	11300
31·0	9	57	40	0·71	13900
38·3	11	55	38	0·86	16000
62·4	11	56	33	1·31	21100

The considerable correspondence between the theoretical and the experimental profiles leads immediately to the question of the degree to which the power law dependence indicated by the theory is borne out by the experimental results. Since that distance is measured from a source at the effective origin of the flow, it must be obtained from a combination of experiment and theory in reference to some feature of the flow and the profiles themselves can be used for this. If the thickness, δ, is specified from equation

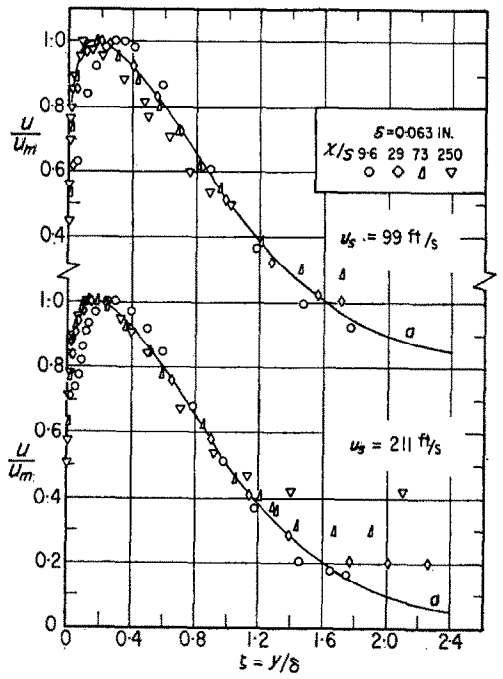

FIG. 4. Velocity profiles for the 0·063 in slot.

The upper set of results is for an injection velocity of 99 ft/s and the lower for 211 ft/s, the slot Reynolds numbers being of the order of 3030 and 6450 respectively. The curves are curve "a" of Fig. 2. Associated quantities are as follows.

x/s	u_1 (ft/s)	u_s (ft/s)	u_m (ft/s)	δ (in.)	$u_m\delta/\nu$
9·6	13	99	107	0·085	4580
29	13	99	69	0·17	6050
73	12	99	47	0·39	9270
250	12	99	28	1·56	22300
9·6	23	211	196	0·10	10100
29	23	211	135	0·20	13600
73	22	211	94	0·43	20500
250	23	211	57	1·44	41700

(4) and the maximum velocity, u_m, from equation (3), then the reference velocity can be eliminated to define the distance ξ; or, equivalently, the (positive) distance from the upstream origin to the slot location.

$$\frac{\xi}{s} = \frac{x}{s} + \frac{x_0}{s} = \left(\frac{\delta}{s}\right)\left(\frac{\delta u_m}{\nu}\right)^{1/4}\left[\frac{4}{0{\cdot}0275}\right.$$

$$\left.\times\left(1 - \frac{4+\alpha}{5+4\alpha}\right)(\alpha + 0{\cdot}07)\eta_t^{-5/4}\left(\frac{f_m}{f'_m}\right)^{5/4}\right]. \quad (6)$$

The function f'_m, f_m, and the distance η_t are given as functions of α in Ref. 3 and the values for x_0/s that are obtained from the profiles of Fig. 3 are contained in Table 1.

Table 1. *Values of* x_0/s, 0·25 *in slot*

From profile at x =	0·208	0·308	1·3
for α = 1·2	13	18	45
1·3	34	50	142

It is clear from the results in the table that the dependence of the upstream distance x_0/s on the parameter α is far too strong in terms of the scant choice in the value of the parameter that can be made from the velocity profiles. A disquieting feature of the tabulated results is the increasing upstream distance that is defined by the profiles at greater downstream distances and consequent implication that a true power law behavior may not exist in the experimental results. Such a situation is possible and may be engendered by the increasing influence of the free stream velocity at large downstream distances, where the maximum velocity becomes low. In any case, equation (6) does not yield consistent results and as an alternative a best fit to a power law behavior was obtained by arbitrary choices of the distance x_0/s. This is not a particularly definitive procedure and a considerable latitude is available in the choice; the value $x_0/s = 12$ was chosen as a magnitude giving the reasonable portrayal contained in Fig. 5. There the experimental values are subject to the empirical generalization of representing $(u_m\delta)/(u_s s)$ and u_m/u_s. This applies fairly for the local value of $u_m\delta$, and the values thereof can be found, within 5 per cent, from the relation

$$\frac{u_m\delta}{u_s s} = 0{\cdot}212\left(\frac{\xi}{s}\right)^{0{\cdot}60}. \quad (7)$$

There is less agreement in the case of the maximum velocity, and in particular the values for the 0·25 in slot reveal a reduced dependence on distance, while those for the 0·063 in slot indicate a small magnitude dependence on the injection velocity. To obtain a single equation,

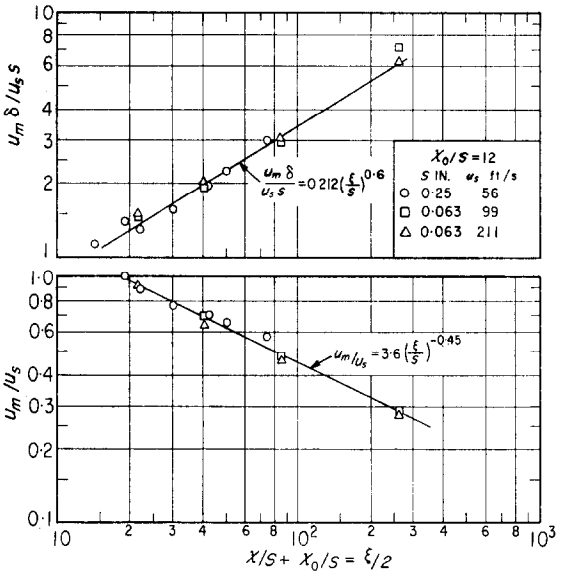

FIG. 5. The maximum velocity and the layer thickness. The curves represent the best fit to the experimental data and are equations (7) and (8).

an approximately 5 per cent tolerance is accepted and the last point for the 0·25 in slot neglected, with the result

$$\frac{u_m}{u_s} = 3{\cdot}6\left(\frac{\xi}{s}\right)^{-0{\cdot}45}. \qquad (8)$$

Table 2 contains the individual results for the exponents a and b, for $u_m \sim \xi^a$ and $\delta \sim \xi^b$, and includes the predictions of these exponents for $\alpha = 1{\cdot}2$ and $1{\cdot}3$ from equations (1) and (2). The experimental values of the exponent "a" are a little low, those of "b" a little high, but the degree of dependence is of the same order as is the selection that is available from equations (1) and (2).

SHEAR COEFFICIENTS

Shear coefficients have been determined from the velocity profiles by a semi-logarithmic representation of the values near the wall and the location of this part of the profile in agreement with the law of the wall, taken as

$$\frac{u}{\sqrt{\tau_0/\rho}} = 5{\cdot}5 + 2{\cdot}5 \log \frac{y\sqrt{(\tau_0/\rho)}}{\nu} \qquad (9)$$

and also with the profile of the transition layer, taken on the Kármán basis as

$$\frac{u}{\sqrt{\tau_0/\rho}} = -3{\cdot}05 + 5 \log \frac{y\sqrt{(\tau_0/\rho)}}{\nu}. \qquad (10)$$

The use of the transition layer velocity distribution for the appraisal of the friction was dictated by the small extent of the region where the law of the wall could be expected to apply, for in most cases the velocity maximum occurred in the region of $y\sqrt{(\tau_0/\rho)}/\nu = 150$ and the influence of the greater diffusivity that existed there was evident in a departure of the velocity profile from equation (9) in that part of the inner layer near the velocity maximum. The uncertainty in the determination of the friction, particularly due to this effect, made the possible error in the coefficients about 5 per cent for the results for the 0·25 in slot and 10 per cent for those for the 0·063 in slot

Figure 6 shows the values, as coefficients, $\tau_0/\rho u_m^2$, presented as a function of the relative distance ξ/s and demonstrates approximately the power law behavior predicted by the theory, in which it was assumed that near the wall

$$\frac{\tau_0}{\rho u^2} = \frac{0{\cdot}0225}{(uy/\nu)^{1/4}}. \qquad (11)$$

If this relation is presumed to hold as far as the velocity maximum then there is indicated a

Table 2. Power law exponents

Slot	u_s	$(a - b)$	a	$(a + b) - a$			a	b
0·250	56	0·60	−0·37	0·97	Equation (1)	$\alpha = 1{\cdot}2$	−0·49	0·90
0·063	211	0·60	−0·45	1·05		$\alpha = 1{\cdot}3$	−0·51	0·90
0·063	99	0·63	−0·47	1·10	Equation (2)	$\alpha = 1{\cdot}2$	−0·55	1
Equations (7, 8)		0·60	−0·45	1·05		$\alpha = 1{\cdot}3$	−0·56	1

proportionality of the shear coefficient to $\xi^{-(a+b)/4}$ and Fig. 6 then demonstrates agreement with the values of the exponent that are obtained from equations (1) or (2). In more specific reference to the experimental results, with δ_m/δ

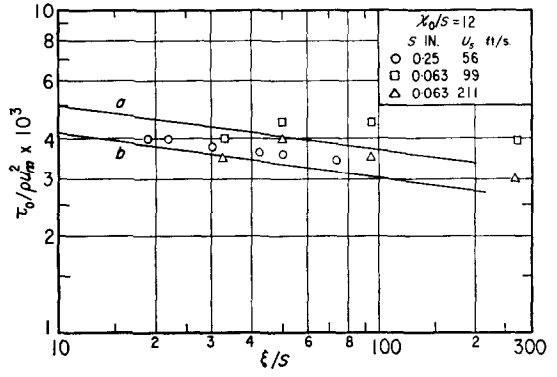

FIG. 6. Skin friction coefficients.

Curves a and b are equation (12) for slot Reynolds numbers of 3500 and 7000 respectively.

taken as 0·18 and equation (7) used for $u_m\delta$, equation (11) becomes

$$\frac{\tau_0}{\rho u_m^2} = \frac{0{\cdot}054}{(u_s s/\nu)^{1/4}} \left(\frac{\xi}{s}\right)^{-0{\cdot}15} \qquad (12)$$

Fig. 6 contains the indication of equation (12) for two values of the Reynolds number that are typical of the experimental values to demonstrate an acceptable correspondence, particularly at the higher Reynolds number. The results for the lower Reynolds number are above equation (12), but the accuracy of these values is particularly questionable.

TEMPERATURE PROFILES

Temperature profiles were obtained with a 40 gage nichrome–constantan thermocouple, mounted on a fork made of sewing needles. Traverses were made with heated injection and an adiabatic wall, for operating conditions similar to those for which the velocity profiles were determined. These temperature profiles are presented as the ratio t/t_a, where t_a is the observed wall temperature and the few instances in which the ratio exceeds unity at the wall reflect discrepancies between the indication of the thermocouple probe and the thermocouple in the wall. Fig. 7(a) presents the profiles obtained for the 0·25 in slot and reveals essential similarity for those profiles at positions at and downstream of $x/s = 18$ ($\xi/s = 30$). This agrees with the indication of the velocity profiles that it is in this region that similarity is first achieved.

All of these profiles are for an adiabatic wall condition but only those for positions very near the slot show a slope of zero at the wall. At the downstream positions for which similarity is attained the curvature of the profile at the wall is so great that the initial slope of zero is not discernable. This feature exists also in the analytical predictions that are presented later.

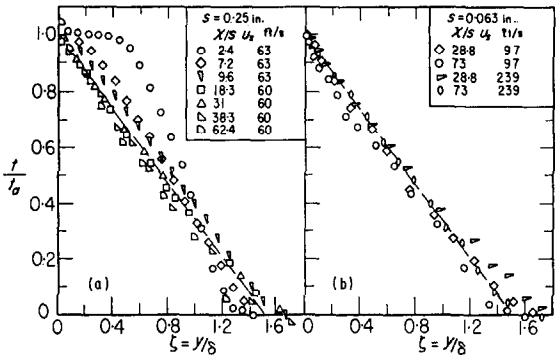

FIG. 7. Temperature profiles.

(a) and (b) show results for the 0·250 and 0·063 in slots respectively. Operating conditions were similar to those for the velocity profiles shown on Figs. 3 and 4. The curve is the mean experimental profile for the 0·250 in slot.

Figure 7(b) presents the few profiles obtained for the 0·063 in slot and also reveals that similarity was attained at least for the first position at $x/s = 28{\cdot}8$. The average experimental curve determined from the profiles for the 0·25 in slot is also shown on Fig. 7(b) and exhibits a good degree of correspondence to the profiles shown on that figure.

Beyond the realization of the expected similarity, the further appraisal of the profiles must deal with the extent to which the theoretical prediction is realized and such a prediction can be made from the hydrodynamic solution if the diffusivities for heat and momentum are taken to be equal. Insofar as the molecular contributions are concerned, this implies of course

a Prandtl number of unity. The energy equation, with dissipation neglected and properties taken as constant, is

$$u\frac{\partial t}{\partial \xi} + v\frac{\partial t}{\partial y} = \frac{\partial\ (\epsilon \partial t/\partial y)}{\partial y}. \qquad (13)$$

With $u/_m u = F'(\zeta)$, where

$$\zeta = \frac{y}{\delta};\ \frac{\epsilon}{\delta[\mathrm{d}(u_m\delta)/\mathrm{d}\xi]}$$

depending only on ζ; and $t = t_a g(\zeta)$ with $t_a \sim \xi^{-(a+b)}$; this equation transforms to the ordinary differential equation:

$$\frac{\mathrm{d}gF}{\mathrm{d}\zeta} = \frac{\mathrm{d}}{\mathrm{d}\zeta}\left[\frac{\epsilon}{\delta[\mathrm{d}(u_m\delta)/\mathrm{d}\xi]}\right]\frac{\mathrm{d}g}{\mathrm{d}\zeta}. \qquad (14)$$

With an adiabatic wall, $\mathrm{d}g/\mathrm{d}\zeta = 0$ at $\zeta = 0$ and

$$\frac{\mathrm{d}g}{\mathrm{d}\zeta} = \left[\frac{\delta[\mathrm{d}(u_m\delta)/\mathrm{d}\xi]}{\epsilon}\right] gF \qquad (15)$$

and since $g(0) = 1$, there is obtained for the temperature profile

$$g = \exp\left\{-\int F\left[\frac{\delta}{\epsilon}\frac{\mathrm{d}(u_m\delta)}{\mathrm{d}\xi}\right]\mathrm{d}\zeta\right\} \qquad (16)$$

Figure 8 shows the profile predicted from the velocity distribution and diffusivity for $\alpha = 1{\cdot}2$ as they are indicated on Fig. 2, except that the "inner" diffusivity was used as far as $\zeta = 0{\cdot}18$. Comparison with the curve that approximates the experimental profile shows that the predicted resistance near the wall is too large and that in the outer layer, beyond the velocity maximum, it is too small. To show how the prediction is affected by the magnitude of the diffusivity, a prediction is also shown for the case in which the diffusivity of the inner layer has been increased by a factor of 1·65 and that of the outer layer has decreased by a factor of 0·77. This agrees with the experimental values in the inner region and it is to be noted that the increase in the diffusivity that has been used is far greater than might be expected from any consideration that the Prandtl number of the air is 0·70. There is an irregularity in the prediction near the velocity maximum that is due to the sudden increase in the postulated diffusivity but the remainder of the

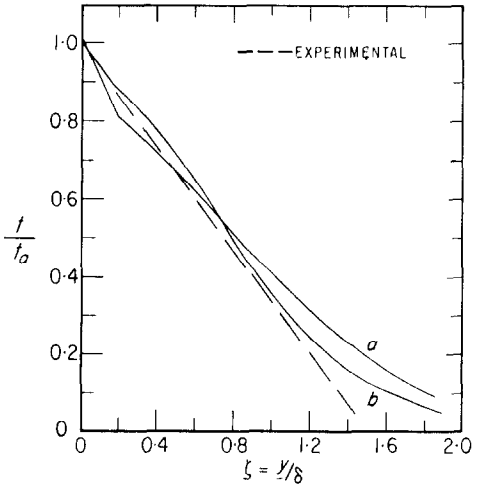

FIG. 8. Temperature profiles.

The experimental curve is that shown in Fig. 7. Curve *a* is that for the diffusivity given by curve *c* on Fig. 2 for $\alpha = 1{\cdot}2$. Curve *b* is that also given by curve *c* on Fig. 2, but with ϵ increased by 65 per cent for $\zeta < 0{\cdot}18$ and decreased 23 per cent for $\zeta > 0{\cdot}18$.

prediction is in accord with experiment out to $y/\delta = 1$. Beyond this, the experimental values themselves are not well represented by the line that is indicated for them, as it is in this region that the existence of the finite free stream velocity apparently diminishes the diffusivity to values below that of the prediction.

Another view of the value of the diffusivity that is needed for better correspondence is presented in Fig. 2, where there has been indicated the diffusivity that would be required for the realization of the linear temperature profile with the theoretical velocity distribution corresponding to $\alpha = 1{\cdot}2$. This of course is obtainable directly from equation (15) in a particularly simple way when the temperature profile is approximated as linear. The diffusivity obtained in this way varies continuously with ζ and in the outer region there is indicated an average value of the order of $\epsilon/\delta\ [\mathrm{d}(u_m\delta)/\mathrm{d}\xi] = 0{\cdot}40$. In the theory the diffusivity in the outer region is presumed to vary only with distance along the plate according to $u_m\delta_t/\epsilon = 1/\kappa$. From equation (5),

$$\kappa = \left[\frac{\epsilon}{\delta[\mathrm{d}(u_m\delta)/\mathrm{d}\xi]}\right]\frac{(a+b)}{0{\cdot}85}\frac{\delta}{\xi},$$

and with equations (7) and (8) used to evaluate δ/ξ and to define $(a + b)$, this becomes

$$\kappa = (0{\cdot}069)\left\{\frac{\epsilon}{\delta[\mathrm{d}(u_m\delta)/\mathrm{d}\xi]}\right\}.$$

This gives $\kappa = 0{\cdot}042$ and $0{\cdot}028$ for

$$\left\{\frac{\epsilon}{\delta[\mathrm{d}(u_m\delta)/\mathrm{d}\xi]}\right\}$$

equal to $0{\cdot}61$ and $0{\cdot}40$ respectively and these values are larger than that of $\kappa = 0{\cdot}012$ inferred by Glauert for the radial wall jet.

EFFECTIVENESS

The effectiveness is the ratio of the local adiabatic wall temperature to the temperature of the injection air, and the observations concerning the similarity of the temperature and velocity profiles imply that the effectiveness should be proportional to $\xi^{-(a+b)}$ at downstream distances greater than ξ/s of the order of 30. Fig. 9 shows the values of the effectiveness to indicate this to be true, and that the individual

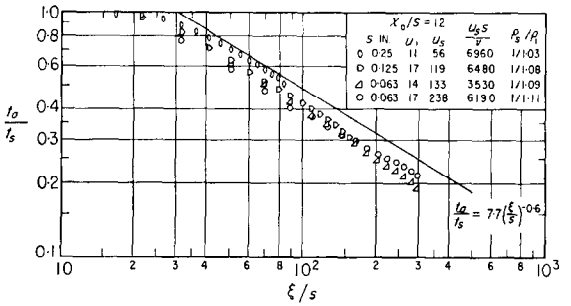

FIG. 9. Effectiveness.
The curve is equation (20) for $\rho_s/\rho_1 = 1{\cdot}0$.

slopes for the three runs illustrated do vary slightly from about $-0{\cdot}60$ for the 0·25 in slot to $-0{\cdot}57$ for the 0·063 in slot with the high speed injection. Table 2 gives $(a + b) = 0{\cdot}60$ for both conditions, as does equation (7).

Further consideration of the effectiveness requires the specification of t_a from an energy balance

$$c_p\rho_s u_s s t_s = \rho_1 c_p u_m t_a \delta \int_0^\infty \frac{\rho}{\rho_1}\frac{u}{u_m}\frac{t}{t_a}\mathrm{d}\left(\frac{y}{\delta}\right). \quad (17)$$

For the relatively small temperature differences involved in the results shown in the figure, for which $T_s/T_1 < 1{\cdot}11$, the integral in equation (17) can be approximated as

$$\int_0^\infty \frac{u}{u_m}\frac{t}{t_a}\mathrm{d}\left(\frac{y}{\delta}\right) - \frac{t_a}{T_1}\int_0^\infty \left(\frac{t}{t_a}\right)^2 \frac{u}{u_m}\mathrm{d}\left(\frac{y}{\delta}\right). \quad (18)$$

The second integral is 0·7 times the first but the coefficient t_a/T_1 is only 0·11 as a maximum, so that the second term of the expression (18) is neglected and equation (17) is approximated in the following form, the denominator then being at most 8 per cent high.

$$\frac{t_a}{t_s} = \frac{\rho_s u_s s}{\rho_1 u_m \delta}\Big/\int_0^\infty \frac{u}{u_m}\frac{t}{t_a}\mathrm{d}\left(\frac{y}{\delta}\right). \quad (19)$$

The integral, evaluated from the linear temperature profile of Fig. 7 and the theoretical velocity profile for $a = 1{\cdot}2$, has a value of 0·607, and if equation (7) is used for the ratio $u_s s/u_m\delta$ there is obtained

$$\frac{t_a}{t_s} = 7{\cdot}7\frac{\rho_s}{\rho_1}\left(\frac{\xi}{s}\right)^{-0{\cdot}60}. \quad (20)$$

There is risk in this formulation because both the velocity profile used in the integral in equation (19) and $u_s s/u_m\delta$ given by equation (7) were obtained for isothermal conditions, and not for the case of variable density now considered. Also, the value of the integral as used in equation (19) is too high, as noted. Thus equation (20) shown on Fig. 9 with $\rho_s/\rho_1 = 1{\cdot}0$ is at least something less than 11 per cent too high for the 0·063 in slot, the difference decreasing with increasing slot size.

HEAT TRANSFER

Temperature profiles were not obtained for the runs made with heat transfer and the consideration is limited to the comparison of the results previously reported to the evidence about the flow that has been presented here. Fig. 10 shows the pertinent runs portrayed in the correlation previously proposed, as a function of the effective distance ξ. This is essentially the portrayal used originally [1] except that the addition of the distance $x_0/s = 12$ eliminates the need in these runs, at least, for the separate correlation that was used for the region near the

slot. But previous evidence here indicates that the power law dependence

$$\frac{h}{\rho_s u_s c_p}\left(\frac{u_s s}{\nu}\right)^{0.3} = 0.41\left(\frac{\xi}{s}\right)^{-0.60} \tag{21}$$

shown on Fig. 10 as curve c, should not be expected closer to the slot than $\xi/s = 30$. Beyond this point the correlation is fairly successful, approximating a power law with a scatter of points in a band about 10 per cent in width.

Contrasted to the effectiveness, the heat transfer depends crucially on conditions near the wall, and the solution of equation (13) will need to be matched to some appropriate sublayer assumptions in order to obtain a proper result. In lieu of this there is chosen here the Colburn analogy,

$$\frac{h}{\rho u_m c_p}(\sigma)^{2/3} = \frac{\tau_0}{\rho u_m^2}$$

as a possible appropriate relation between the heat transfer and friction coefficients. If this choice is combined with equations (12) and (8), there is obtained the relation

$$\frac{h}{\rho u_s c_p} = \frac{0.25}{(u_s s/\nu)^{1/4}}\left(\frac{\xi}{s}\right)^{-0.60} \tag{22}$$

Fig. 10 shows that the prediction of equation (22) is not more than 10 per cent low and that the effect of the difference in the exponents of the slot Reynolds number in equation (22) and the correlation used on Fig. 10 is not a crucial one in the range of Reynolds numbers that is encompassed there. It is noteworthy that the correspondence between the thermal and the hydrodynamic behavior that is achieved for this flow is the equal of that usually found for the more conventional systems of pipe flow and the usual turbulent boundary layer on a plate.

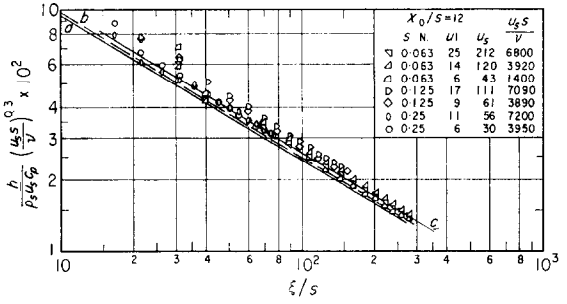

FIG. 10. Heat transfer.

Curves a and b are equation (22) for slot Reynolds numbers of 3000 and 6000 respectively. Curve c is equation (21).

SUMMARY

An approximation to the wall jet, in which the free stream velocity was small but not zero, has been investigated experimentally to appraise the degree to which the behavior of the theoretical flow was realized and to establish the extent to which the measured effectiveness and heat transfer coefficient might be predicted. Generally successful achievement of these comparisons embraced the following items.

The velocity profile in that system considered is practically the same as that predicted and this correspondence holds almost to the point at which exists the free stream velocity; and this agreement existed beyond about 18 slot heights downstream of the slot. Power law behavior exists approximately with respect to downstream distance with exponents being of the order of magnitude that are indicated by the theory, but this is the weakest part of the comparison. The friction factors can be predicted well if the experimental dependence on distance is employed.

Agreement between the predicted temperature profiles and those determined experimentally with an adiabatic wall requires some alteration of the eddy diffusivity and in particular the value in the outer region must be reduced by 30 per cent from that implied by the theory; but other than this, the correspondence is perhaps better than would have been anticipated. When values of the effectiveness are predicted from the hydrodynamic and thermal profiles the prediction agrees with the results for the larger slot but is otherwise high by about 15 per cent.

Heat transfer coefficients, predicted from the flow results, are about 10 per cent below the data; and the prediction, based upon the Colburn analogy, verifies this relation for this system.

ACKNOWLEDGEMENT

The research which yielded these results was supported by the National Science Foundation under Grant G-10171.

REFERENCES

1. R. A. SEBAN, Heat transfer and effectiveness for a turbulent boundary layer with tangential fluid injection. *Trans. Amer. Soc. Mech. Engrs, J. Heat Transfer*, C **182**, 303 (1960).
2. M. JAKOB, R. ROSE and M. SPILMAN, Heat transfer from an air jet to a plane plate with entrainment of water vapor from the environment. *Trans. Amer. Soc. Mech. Engrs*, **72**, 859 (1950).
3. M. B. GLAUERT, The wall jet. *J. Fluid Mech.* **1**, 525 (1956).
4. A. SIGALLA, Experimental data on a turbulent wall jet. *Aircr. Engr*, **30**, 131–134 (1958).